Utilizing Algae Produced Astaxanthin to Block UVA Radiation

Mansi Kothari, Jaime Levy

Abstract—**While the protection provided by sunscreen is undeniable, the use of sunscreen holds many consequences for our bodies and the environment. The toxins in sunscreen such as homosalate, oxybenzone, octinoxate, octocrylene, and titanium dioxide disrupt the ocean's ecosystem and the human endocrine system. Our study focuses on the use of an antioxidant called astaxanthin as an effective alternative. Astaxanthin has been renowned as "king of antioxidants," recognized for its beneficial properties on the skin such as anti-aging effects, increased elasticity, increased moisturization, and, most important to our study, its potential to block ultraviolet radiation (UVR). We performed our experiment by measuring the intensity of UVR that passed through controlled amounts of both astaxanthin and sunscreen and found that astaxanthin is as effective in blocking UVR as sunscreen. Our results led us to further our experimentation by combining the astaxanthin with cocoa butter to form a topical application product. These results allow astaxanthin to be considered as both a safer and superior alternative to sunscreen, as astaxanthin does not contain the toxins present in sunscreen and is beneficial to the skin.**

I. INTRODUCTION

Human activity is deteriorating Earth's natural beauty at unprecedented rates, greatly contributing to global temperature rise along with several other environmental effects. Along with the increase in UVR exposure comes increased protection against the harmful rays. Sunscreen, the most common form of sun protection, is used by 68.1% of adults aged 41-64 and 79.7% of adolescents aged 12-20, according to a sample survey we conducted. While sunscreen does prove beneficial in blocking UVR, it contains toxins that are harmful to the body. These toxic substances include homosalate, oxybenzone, octinoxate, octocrylene, and titanium dioxide, which penetrate the skin and cause endocrine disruption and cell damage.[1,2] The increased use of sunscreen also contributes to pollution through coral bleaching, a process which disrupts the symbiotic relationship between coral and algae.[3] When coral rejects symbiotic organisms, it cannot survive and this has a direct correlation to the increased concentration of CO_2 in the air as coral absorbs CO_2.[4] The increase in CO_2 leads to global warming and climate change.
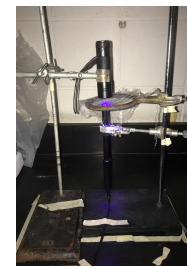
Considering the widespread use combined with the undesirable effects on both the human population and the environment, sunscreen should not be regarded so highly when there is an alternative out there: astaxanthin. Astaxanthin, an antioxidant produced mainly by Haematococcus pluvialis, microalgae, has shown to have many beneficial qualities on the skin, such as anti-aging effects, increased skin moisture, elasticity, and through limited research, has been shown to be a possible protector from UV radiation.[5,6] However, astaxanthin has only been

used commercially as a dietary supplement, and has very limited testing as a topical application because of its lack of water solubility.[7] This limits the extent to which astaxanthin can benefit people in protecting themselves against UV radiation because topical applications provide a more targeted and efficient supply to the skin.[6] It was hypothesized that astaxanthin is just as effective as sunscreen in blocking UV radiation. We sought to then formulate a topical application that can be used as an alternative to sunscreen.

II. METHODS

Experimental Setup:

A clamp was placed 15 cm high on one ring stand and a second clamp was placed 10 cm high on a second ring stand. A third ring clamp was placed 5 cm above the second clamp on the second ring stand. Next, a UV lamp was attached to the clamp on the first ring stand and a UV sensor to the clamp on the second ring stand, pictured in Figure 1. To emulate direct sunlight exposure, two ring stands were positioned so that the UV lamp was directly above the UV sensor and in the center of the ring clamp. To ensure

Figure 1: *Experimental setup used to conduct experiment*

precision, tape was placed around the original setup, since the UV sensor is very sensitive to movement. This setup allowed the efficiency of both astaxanthin and sunscreen to be tested with as much accuracy and precision as possible.

Preparation:

First, the intensity of UV radiation present in the room of experimentation was recorded. Then, plastic wrap was cut into twenty twelve by twelve cm squares and ten were labeled 1A through 10A and the other ten 1B through 10B. The intensity that passed through only plastic wrap was then recorded to be accounted for in our data. Next, the density of the sunscreen was calculated by taking the mass of 1 milliliter of sunscreen in a pipette. Knowing the density allowed equal amounts of astaxanthin and sunscreen to be used since astaxanthin was measured in volume, since it is liquid, while mass was used for sunscreen, since it is viscous. After taking preliminary measurements, squares 1A through 10A were assigned to represent astaxanthin, and squares 1B through 10B to represent sunscreen.

Application:

Using a pipette, one milliliter of astaxanthin was dropped onto square 1A directly above the sensor, and then the UV intensity that passed through the astaxanthin was recorded using a Vernier LabQuest attachment to the UV sensor. We then repeated this procedure for squares 2A through 10A.

Next, 1.5 grams of sunscreen were evenly spread onto square 1B directly above the sensor and the UV intensity that passed through the sunscreen was recorded. This procedure was repeated for squares 2B through 10B.

III. RESULTS AND DISCUSSION

Through the utilization of our experimental setup, we assessed the ability of both sunscreen and astaxanthin to block UVR. It was found that on average, astaxanthin and sunscreen block about the same percentage of UVR, except for one outlier in one of the sunscreen trials. Both astaxanthin and sunscreen blocked between 99.8 and 99.9 percent of the UVR. These results led us to proceed further and investigate possible options for creating a topical application.

Table 1: Quantitative Difference in Radiation Blocked					
Trial	Sunscreen (mW/m²)	Astaxanthin(mW/m²)	Difference	% Blocked (Asx)	% Blocked (Sunscreen)
1	53.0	27.0	-26.0	0.999	0.997
2	40.0	31.0	-9.00	0.998	0.998
3	38.0	32.0	-6.00	0.998	0.998
4	28.0	28.0	0.0	0.999	0.999
5	27.0	27.0	0.0	0.999	0.999
6	28.0	27.0	-1.00	0.999	0.999
7	27.0	27.0	0.0	0.999	0.999
8	28.0	28.0	0.0	0.999	0.999
9	28.0	28.0	0.0	0.999	0.999
10	31.0	28.0	-3.00	0.999	0.998
Avg.	32.8	28.3	-4.50	0.999	0.998
St. Dev	8.50	1.77	8.17	0.0000905	0.000435
St. Error	2.53	0.63	2.53	0.0000286	0.000138

Table 1: Data table represents raw data taken for sunscreen and astaxanthin in all trials. Statistical analysis was performed which shows the validity of the data.
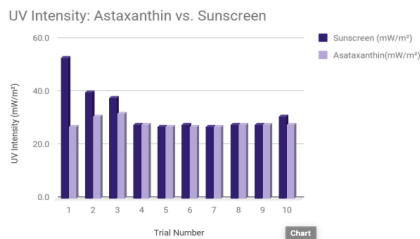

Figure 2: Graph representing the difference in UV intensity that passed through astaxanthin and sunscreen in each trial. It shows that less or equal amounts of UV radiation pass through sunscreen than astaxanthin.

Through further inspection of our data, the trials were mostly consistent and representative of the true mean. This was confirmed by the low standard deviation and standard error. However, the standard deviation and standard error were higher for the sunscreen than the astaxanthin because of an outlier. We suspect that the outlier present was caused by spreading the sunscreen too thin, allowing more UVR to pass through the thinner layer of sunscreen. Although this outlier was present, its effect on the percentage blocked was negligible, and in turn, the difference in percentages for standard deviation and standard error were also negligible. The small standard error allowed us to confirm that the data we collected was representative of the population. These results led us to investigate a method to create an astaxanthin product. Since astaxanthin alone has a red pigment and leaves a stain on the skin, we sought to dilute this effect by mixing it with another product. However, astaxanthin's nonpolar structure contributes to its immiscibility, limiting our options to hydrophobic solutions. We decided to use cocoa butter, a common lipid based substance often used for cosmetic purposes. After melting cocoa butter, mixing it with astaxanthin, and then allowing it to harden, we had created a

"sun stick" which could be used topically on the skin. Our results indicate that this "sun stick" will be just as effective in blocking UVR as sunscreen, and will also provide benefits to the skin.

IV. CONCLUSION

The findings generated in this multifaceted investigation provided insight on the efficiency of astaxanthin in blocking UVR compared to commercial sunscreen, thus affirming our hypothesis that astaxanthin is a viable alternative to sunscreen. After assessing the quantitative results of our experimentation, we also acknowledged the qualitative properties of both astaxanthin and sunscreen. We concluded that astaxanthin is not only a viable alternative, but is potentially a better option due to its superior qualitative properties, such as its anti- aging effects and lack of toxins. The shift from sunscreen to astaxanthin will reduce the amount of sunscreen being used, thus decreasing its consequences on the ocean and the endocrine system.

V. ACKNOWLEDGMENT

VI. REFERENCES

[1] EWG. EWG's 2017 Guide to Safer Sunscreens [Internet]. EWG. [cited 2018Mar27]. Available from: https://www.ewg.org/sunscreen/report/the-trouble-with-sunscreen-chemicals/#.Wrp1 of wUdU

[2] Shaffer LSL, DavidWolfe.com. 6 Dangerous Sunscreen Ingredients You Need To Watch Out For! [Internet]. DavidWolfe.com. 2017 [cited 2018Mar27]. Available from: https://www.davidwolfe.com/6-dangerous-sunscreen-ingredients/

[3] Downs CA, Kramarsky-Winter E, Segal R, Fauth J, Knutson S, Bronstein O, et al. Toxicopathological Effects of the Sunscreen UV Filter, Oxybenzone (Benzophenone-3), on Coral Planulae and Cultured Primary Cells and Its Environmental Contamination in Hawaii and the U.S. Virgin Islands. Archives of Environmental Contamination and Toxicology. 2015;70(2):265–88.

[4] Tovar-Sánchez A, Sánchez-Quiles D, Basterretxea G, Benedé JL, Chisvert A, Salvador A, et al. Sunscreen Products as Emerging Pollutants to Coastal Waters [Internet]. PLoS ONE. Public Library of Science; 2013 [cited 2018Apr13]. Available from:https://www.ncbi.nlm.nih.gov/pmc/articles/PMC3673939/

[5] Worland J. Why Coral Reefs Are Dying: Sunscreen Killing Reefs [Internet]. Time. Time; 2015 [cited 2018Apr13]. Available from: http://time.com/4080985/sunscreen-coral-reefs/

[6] Cheng W, Rosprim D. A Red Miracle for Skin Health [Internet]. DERMASCOPE Magazine. [cited 2018Mar27]. Available from: https://www.dermascope.com/ingredients/a-red-miracle-for-skin-health

[7] Hama S, Takahashi K, Inai Y, Shiota K, Sakamoto R, Yamada A, et al. Protective Effects of Topical Application of a Poorly Soluble Antioxidant Astaxanthin Liposomal Formulation on Ultraviolet-Induced Skin Damage. Journal of Pharmaceutical Sciences [Internet]. 2012;101(8):2909–16. Available from: https://www.ncbi.nlm.nih.gov/pubmed/22628205
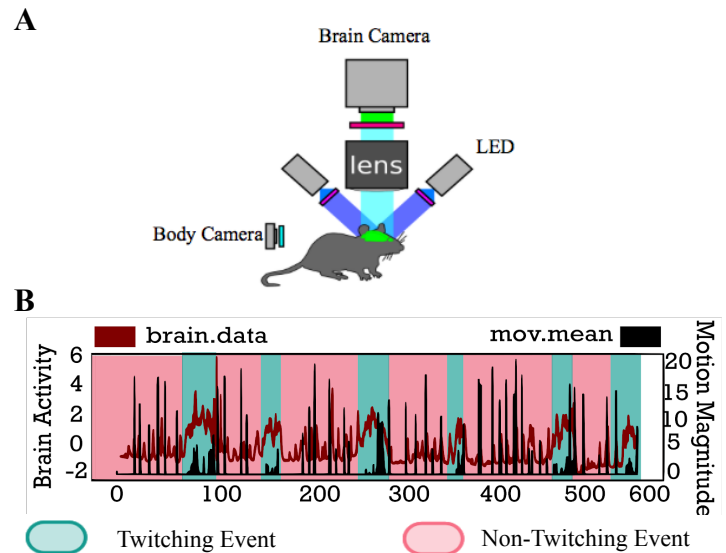
Identifying Behavioral Movements of a Mouse Using Machine Learning

Shreya Mantripragada, Emma Dionne, and Jimmy Chen

Abstract— **In developmental neuroscience, there is a need to understand how state plays an active role in the developing brain. This paper presents a novel approach of using machine learning techniques to distinguish two states in early postnatal mice, twitch and non-twitch occurrences, using information from its gross brain activity and body camera recordings. Supervised machine learning was initially done to help gain insight into associations between human classifications and the training metrics. However, the goal of the work was to come up with an accurate unsupervised machine learning technique [2] that closely represented the results of the human classification. Throughout this process, data reduction and clustering techniques were used to develop this unsupervised machine learning algorithm. Results were then validated against the human classification resulting with an accuracy of 82.6%. These initial results will allow researchers to use our algorithm as a starting point to test machine learning algorithms on other behavioral states occurring in a variety of animals, furthering our understanding of the principal connections between the brain and body.**

I. INTRODUCTION

The human brain controls, monitors, and regulates an individual's bodily functions. To establish proper functions, developmental brain waves help to link the body function to the complex brain structures. These processes of the brain's development from neonate to adult are vaguely understood. It is hypothesized that sleep cycles are necessary for perinatal brain development, a vital stage in which the brain forms and develops proper connections, aiding in memory and brain functionality [1]. Due to the structural and functional similarities between a human brain and a mouse's brain [1], we can begin to look at emergent developmental patterns in perinatal mice. To do this, we recorded from postnatal day 7 mice brain activity, through pan-neuronal expression of a genetically encoded calcium indicator, while recording body movements (Fig. 1A). We identified periods of time when the mouse pup displayed signs of *active-sleep*. During these *active-sleep* periods, mice undergo a series of unconscious movements throughout the body, classified as twitching events. The average brain activity across the neocortex was taken to represent the distinct mental states. The behavioral data was processed using Optic Flow functions that approximate the amount of motion that occurs between two subsequent frames. When we juxtapose the average brain activity with the average motion, we noted the time frames of twitching (small motions with short inter-event time-lag) aligned with high amounts of brain activity (Fig. 1B, blue periods). This direct relationship of twitching events in the mouse's body with high neurological activity is the relationship we sought to explore using machine learning applications.
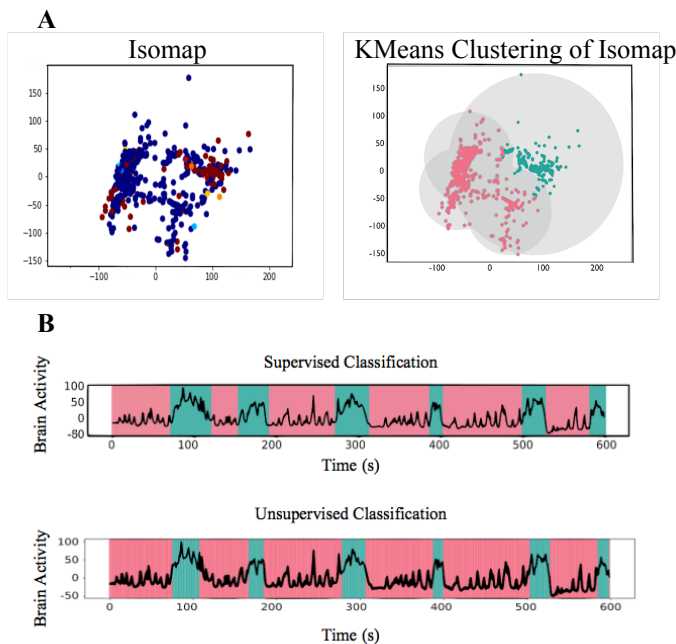

A

B

Figure 1A: *The experimental setup on the mouse in order to receive its body movements and brain activity through cameras that were placed next to the mouse's body and above its brain.*

Figure 1B: *Average brain activity (maroon line) on top of the average movement data (black line) showed the two distinct states of which we call twitch (blue periods) and non-twitch (pink periods).*

II. METHODS

The initial pieces of data were the mouse's neural signals and physical body movements. From these two metrics, the list was expanded to over 30 different features by taking mathematical derivations and operations (ie: derivatives, ranges, windowed standard deviations, etc.) of the initial two metrics. This expanded list of metrics was narrowed down to metrics that allowed for good separation of twitching and non-twitching events, based on human classification. We visualized this separation through pairplot graphs, which plotted each of the metrics against all other metrics. From these pairplots, we selected 4 metrics that best distinguished the two states, and these 4 chosen metrics were then reduced into two dimensions using dimension reduction algorithms such as t-SNE and isomap. Dimensionality reduction creates a new copy of the data and reduces the data-set from 4 to 2 dimensions, allowing us to better visualize the numerical information. Further, we utilized the reduced dimension dataset to cluster our input data to two states. The dimensionality reduction technique that proved to be the best for clustering was KMeans (Fig. 2A). Once those instances were classified, a clean-up algorithm was created for the unsupervised classifications to eliminate the outliers and clearly classify complete twitching events. Due to the

success of the KMeans Clustering Algorithm, the four metrics were plotted over the brain activity and, as shown by Fig. 2B, were successful in classifying the number of twitching movements, as well as their general duration. Due

to the similarities between our Unsupervised Machine Learning output to the Supervised Machine Learning result, where the specific time series values of the twitch events were inputted, the four metrics chosen were proven to be successful.

A

B

Figure 2A: The leftmost figure displays an isomap dimension reduction of all human classified data points, distinguishing twitching (red dots) and non-twitching (blue dots) occurrences. The rightmost figure shows KMeans clustering on the isomap with the unsupervised clustering classification of twitches (light blue) and non-twitches (pink).

Figure 2B: Comparison between the supervised classification and the unsupervised classification, with twitch periods (light blue) and non-twitch periods (light pink).

III.   RESULTS

After testing the different dimensionality reduction methods and clustering algorithms on our unsupervised machine learning, isomap dimensionality reduction and KMeans clustering proved to be the best means of classifying the two states, twitch and non-twitch. Even though the unsupervised classifications were not perfect, a quick clean-up algorithm perfected the classifications and captured the distinction between the two states, resulting in an improved final accuracy of 82.6%. In comparison, the supervised learning resulted in an accuracy of 94.0%. While the unsupervised learning underperformed in accuracy, the unsupervised learning had only a 11.4% difference.

IV.   DISCUSSIONS

In this study, we set the goal to develop an unsupervised learning algorithm that could detect two distinct states, twitch vs non-twitch, of a developing neonate mouse based on gross neocortical activity and movement data. Identification of the periods in which there is purported active sleep (twitch state) will help developmental neuroscientists to study the emergence of properly functional networks and highlight the importance of these necessary periods for the developing system. We have successfully demonstrated that an unsupervised machine learning approach can be used to identify these periods. Future researchers can build off of these concepts to better implement machine learning to complicated biological processes, using both neural activity and behavior.

V.   ACKNOWLEDGEMENTS

VI.   REFERENCES

1.   Snyder, J. M., Hagan, C. E., Bolon, B., & Keene, C. D., "Comparative Anatomy and Histology," *PDF*, 2nd ed., 2017, pp. 403-444.
2.   Aurélien Géron, "Hands-On Machine Learning with Scikit-Learn & TensorFlow, " *Paperback*, 1st ed. vol. 1, O'Reilly Media Inc, 2017.

The Separation of Metal Ion from Heavy Metal Ion Mixture by "Alginate-Liquid Filter"

Jiung Nam

Abstract— **Heavy metal removal through precipitation result in a toxic sludge that creates many environmental liabilities. This paper details a heavy metal filtration device without such liabilities making usage of electrophoresis and sodium alginate to extract and divide heavy metals in wastewater. Alginate, derived from brown seaweed, has the property of forming a hydrogel with bivalent cations and trapping them in place. Each bivalent cation has different levels of affinity with alginate, gelating at different concentrations of alginate solution. From this discovery, a system capable of separating multiple different metal elements within wastewater in alginate solutions of different concentration was created.**

I. INTRODUCTION

Conventional heavy metal removal in wastewater involves chemical precipitation in which a precipitation reagent such as activated carbon is used to attract the metal ions into a thick sludge. This process includes many drawbacks; a lot of water is lost, the sludge releases harmful dust when dried, the toxic sludge is often disposed in landfills due to a lack of purpose, and most of all, the metal particles within the sludge cannot be retrieved or refined for reusage.[1] Alginate, a polysaccharide mainly found in brown seaweed, has a property of forming a hydrogel with metal ions through ionic cross-links. The method of alginate application in wastewater treatment currently being tested is similar to that of conventional precipitation- alginate is poured into wastewater, after which it forms a gel containing all the various metals within the wastewater like how sludge would form. Similarly, the metal ions within the gel are all clumped together and cannot be refined for reuse.[2] However, each metal element was found to have a different level of affinity towards alginate, or tendency to form a gel with alginate.[3] From this it was predicted that it was possible to create a wastewater treatment system that removed and separated each metal element in different alginate concentrations, which would allow for easier recycling of heavy metals within wastewater.

II. METHODS

A solution containing metal ions was placed in the anode side of an electrophoresis machine. 4 different metal ions were tested; Copper, Cobalt, Nickel and Iron. They were tested both individually and in combinations of up to 3 elements. In between, alginate solutions of different concentrations (0.25%, 0.5%, 0.75%, 1%) were placed in increasing order from the anode towards the cathode. On the cathode side, a solution of sodium acetate was placed to make electrophoresis possible. The alginate solutions, the metal solution, and the sodium acetate solution were separated through paper filters; these would minimize the liquids from mixing, while allowing for metal ion passage throughout the system. The system was given a voltage of 80V to transport the metal ions through the alginate liquid filter.

III. RESULT AND DISCUSSION

In order to test the different levels of affinity, 15ml of 10mM solutions of different metal ions were dropped on a petri dish containing 50ml of 1% sodium alginate liquid. When dropped in a solution of 1% alginate liquid, each metal ion formed a hydrogel of unique quality due to the differences in their affinity towards alginate. Mg^{2+} was not able to form a gel at all, Fe^{2+} and Mn^{2+} formed a viscous liquid, Ni^{2+} and Co^{2+} formed a loose slime, Cu^{2+} and Ca^{2+} formed a thick, tensile jelly. It seemed that the stronger the affinity of the element towards alginate, the more firm the resulting gel was. These results were slightly different from the affinities of each metal element measured by Idota et. al in 2016 [1]. It was predicted that this variation in affinity was caused by differences in the composition of the alginate used for our experiment. Whereas Idota et. al utilized alginate consisting solely of guluronic acid segments (G blocks), alginate with both mannuronic acid segments (M blocks) and G blocks, a characteristic of naturally harvested alginate, was used for the purposes of this experiment.
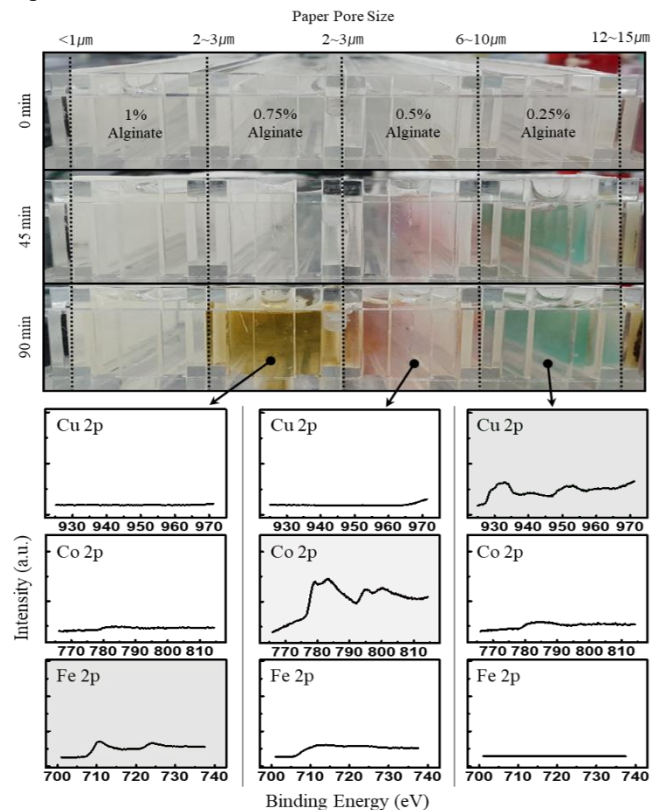

Figure 1. A mixture of Cu^{2+}, Co^{2+} and Fe^{2+} ions were separated in different alginate concentrations over 90 min. (Upper) XPS data showed that each gel possessed high concentrations of only its respective element. (Lower)

The effect of the pore size of the paper filters used to separate the liquids was also tested. 3 different pore size conditions (12~15um, 6~10um, and 2~3um) were tested. Results showed that while pore sizes did affect the rate at which metal ions were transported, they had little effect on the actual separation of metal elements. The smaller the pore sizes, the slower the separation process was. It was predicted that a smaller pore size resulted in less ions being able to pass the paper at a given time, thus slowing the process. In short, it was clear that affinity levels toward alginate had a larger effect on element-based separation compared to the pore size of the paper filters.

A variation in alginate concentrations resulted in a significant level of metal ion division. Initially, each metal was individually tested through the system to verify where they would normally gelated. Cu^{2+} ions mainly gelated within the 0.25% alginate solution, Co^{2+} ions gelated within the 0.5% alginate solution, and Fe ions gelated within the 0.75% alginate solution. Then, a solution including a combination of Cu^{2+}, Co^{2+}, and Fe^{2+} was clearly divided after 90 minutes within the system. Results showed a clear separation amongst the different metal elements, with each alginate concentration displaying high levels of their respective elements. To confirm this separation, an XPS analysis of each of the hydrogels formed by the experiment was conducted. The analysis showed that the elements had indeed been separated, with each concentration showing a high amount of their corresponding element. (Fig. 1)

Elements with weaker affinity towards alginate could only gelate in higher alginate concentrations. These results showed the viability of a heavy metal filtration device capable of element-based separation using variations in alginate concentration. Due to being limited to 4 different concentrations with broad differences (0.25%, 0.5%, 0.75% 1%), it was difficult to distinguish metal elements with comparatively mild differences in affinity. For example, the separation of Cobalt and Nickel was difficult as they both gelated at 0.5% alginate solution, at which the difference in the location of their hydrogels was ambiguous. It was believed that if a metal filtration system that separates a large variety of different metal elements thoroughly with little error was to be created, the affinities of each element towards alginate and the exact concentration in which they would begin gelation must be quantified beforehand. Proper quantification of affinities would allow for the designing of a model that could be applied to more large-scale treatment facilities and other practical purposes.

Metal ions within the hydrogels could be retrieved through the addition of sodium citrate, which liquefied the gel and freed the encapsulated metal ions. A spectrophotometer was used to measure the amount of Cu^{2+} within a liquefied Cu^{2+} hydrogel, then compared with the original amount of Cu added to the alginate solution. Results showed a retrieval of roughly 80% of the original Cu^{2+} within the hydrogel.

IV. Conclusion

A wastewater metal filtration system utilizing alginate capable of complete element-based separation would be a great boon in both environmental and economic perspectives. It would be easy to retrieve the water from the hydrogels as alginate hydrogels can be dried very easily and thoroughly. No harmful dust would be produced, and even if the gels were to be disposed they would be biodegradable, doing comparatively less harm to the environment than sludge.[4] However instead of being disposed the gels can be liquefied using sodium citrate and the metal ions can be retrieved and reused for industrial purposes as they are not mixed. This ability would reduce the amount of heavy metals being disposed into the environment, and make the usage of such materials more economically sustainable for companies. The remaining residue, formed from alginate and sodium citrate, would do little harm even if disposed.

To maximize the potential of such a system, it is necessary to design a device that provides a wide and subtle variation of alginate concentration to separate mixtures with elements sharing similar affinities towards alginate. In addition, a method to accurately quantify each metal element's affinity towards alginate needs to be formulated in order to effectively separate specific elements. Last but not least, the system needs to be tested for application in real conditions. Wastewater from industrial plants must be tested within the device to verify its practicality in separating and recycling heavy metal wastes.

References

[1] Malwina Tytła, "Assessment of Heavy Metal Pollution and Potential Ecological Risk in Sewage Sludge from Municipal Wastewater Treatment Plant Located in the Most Industrialized Region in Poland—Case Study", *Int. J. Environ. Res. Public Health*, 2019, 16, 2430

[2] Matthew Kube, Arash Mohseni, Linhua Fan, Felicity Roddick, "Impact of alginate selection for wastewater treatment by immobilised Chlorella vulgaris", *Chemical Engineering Journal*, vol. 358, 15 February 2019, pp. 1601-1609

[3] Idota, Kogure, Kato, Yano, Arakawa, Miyajima, Ogihara, "Relationship between Physical Parameters of Various Metal Ions and Binding Affinity for Alginate", *Biological & Pharmaceutical Bulletin*, vol. *39,* Issue 11, 2016, pp. 1893-1896.

[4] Bing Wang, Yongshan Wan, Yuling Zheng, Xinqing Lee, Taoze Liu, Zebin Yu, "Alginate-based composites for environmental applications: a critical review", *Critical Reviews in Environmental Science and Technology*, vol. 49, Issue 4, 2019, pp. 318-356

Deciphering genome-wide association studies in Alzheimer's disease

Saloni Shah, Dr. Sarah Morgan, and Dr. Winston Hide

Abstract— **Genome-wide association studies (GWAS) are a hypothesis-free means to identify associations between genetic regions (loci) and characteristics (including diseases). These have been performed on thousands of patients with Alzheimer's disease (AD) in order to find mutations that alter disease risk. In this work, we collect loci identified from GWAS and fine map each locus with the aim of identifying the likely causal variant and therefore understand the mechanisms of AD.**

I. INTRODUCTION

From a metanalysis of genome-wide association studies (GWAS) conducted on Alzheimer's disease (AD) patients [1], 41 disease-associated loci have been identified [2]; the APOE locus is the strongest signal [3] of these 41. Apart from APOE, scientists do not currently believe that the leading variant (i.e. it has the lowest P-value) identified in each locus is the causal mutation, this is only the case 30-60% of the time. Since variants, also known as single nucleotide polymorphisms (SNPs), are inherited together (producing a phenomenon known as linkage disequilibrium, or LD), a nearby variant can serve as a marker for the actual mutation that alters AD risk. In order to identify the likely causal variants for AD, we fine mapped each locus. By doing so, we hope to elucidate the underlying mechanism of disease risk and pave the way to new treatments for AD.

II. METHODS

As shown in our pipeline in Figure 1, we began by gathering the leading SNPs from various papers that analyzed GWAS producing 41 leading AD SNPs. We then found the SNPs in LD with these 41 leading SNPs by using two web tools, LDproxy [4] and Ensembl [5]. After combining the lists and removing any overlaps, we identified a list of approximately 1000 possible SNPs. Next, we annotated the genes that these SNPs associate with using the tool ANNOVAR. This produces an output of annotations, including gene details such as distance and function of the genes. We then used EnrichR [6], a tool that utilized different databases, including Gene Ontology, to understand what functions and pathways the genes are enriched in and how that may have influenced an altered risk for AD, as shown in Figure 2. We also utilized the RegulomeDB score [7] to categorize the SNPs by molecular data; we compared the highest ranked variants (best P-values) to the lowest ranked variants (poor P-values) through a comparison of statistical annotations to observe any differences in function amongst these SNPs, as shown in Figure 3.
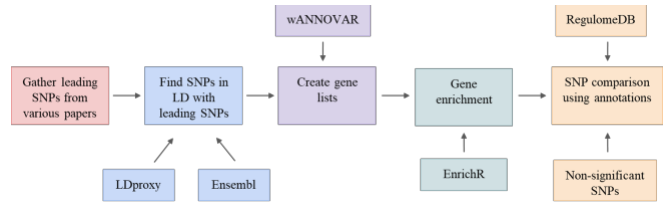
Figure 1: *Method pipeline using leading SNPs to see if SNPs in LD with the leading SNPs were causal variants for AD.*

III. RESULTS AND DISCUSSION

After utilizing the EnrichR tool, we found that two pathways amongst the gene list had a significant P-value: negative regulation of amyloid precursor protein and the negative regulation of amyloid-beta formation. These pathways are critical in identifying a brain that is affected by AD. However, the P-value was more significant for the list consisting of only leading SNPs than of SNPs in LD with the leading SNPs; this means that leading SNPs are more likely to be the causal SNP which is in-line with previous work. Furthermore, from the RegulomeDB scoring, we found that the top ranked SNPs were more commonly eQTLs, which suggests that they change gene expression, showing that the top ranked SNPs were more commonly functional than the bottom ranked SNPs. Nevertheless, some of the top ranked SNPs that we identified had not previously been correlated to AD. We are currently working on identifying the specific SNPs from this list of top ranked SNPs that are likely to alter AD risk by using these annotations to predict causality.
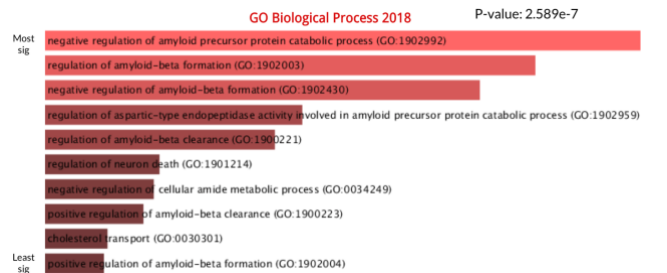
Figure 2: *The top two pathways, negative regulation of amyloid precursor protein catabolic process and regulation of amyloid-beta formation, are significantly enriched in the genes associated with the leading loci (including those in LD). However, these pathways are more significant for the leading SNPs than for all SNPs, showing that leading SNPs are more likely to be the causal SNPs.*

Description	RegDB score	Highest Ranked SNPs	Lowest Ranked SNPs
eQTLs+	1s	3.7%***	0.4%
TF binding+	2s	13%***	8%
	3s		
	4		
TF binding/DNase	5	18%	23%
Other	6	29%	27%
None	No score	29%	34%

*** adjPval < 0.0001

Figure 3: *Highly ranked SNPs are more likely to be eQTLs and transcription factor binding sites. This means that they are more commonly functional than the lowest ranked SNPs.*

IV. ACKNOWLEDGMENT

V. REFERENCES

[1] Jansen, Iris E., et al. "Genome-wide meta-analysis identifies new loci and functional pathways influencing Alzheimer's disease risk." (2019).

[2] Kunkle, Brian W., et al. "Genetic meta-analysis of diagnosed Alzheimer's disease identifies new risk loci and implicates Aβ, tau, immunity and lipid processing." Nature genetics 51.3 (2019): 414.

[3] Lambert, Jean-Charles, et al. "Meta-analysis of 74,046 individuals identifies 11 new susceptibility loci for Alzheimer's disease." Nature genetics 45.12 (2013): 1452.

[4] Machiela MJ, Chanock SJ. LDlink a web-based application for exploring population-specific haplotype structure and linking correlated alleles of possible functional variants. Bioinformatics. 2015 Jul 2. PMID: 26139635.

[5] Zerbino et al. Ensembl 2018. PubMed PMID: 29155950. doi:10.1093/nar/gkx1098

[6] Chen EY, et al. Enrichr: interactive and collaborative HTML5 gene list enrichment analysis tool. BMC Bioinformatics. 2013;128(14)

[7] Amber, Sanila, and Saadia Zahid. "Data integration for functional annotation of regulatory single nucleotide polymorphisms associated with Alzheimer's disease susceptibility." Gene 672 (2018): 115-125.
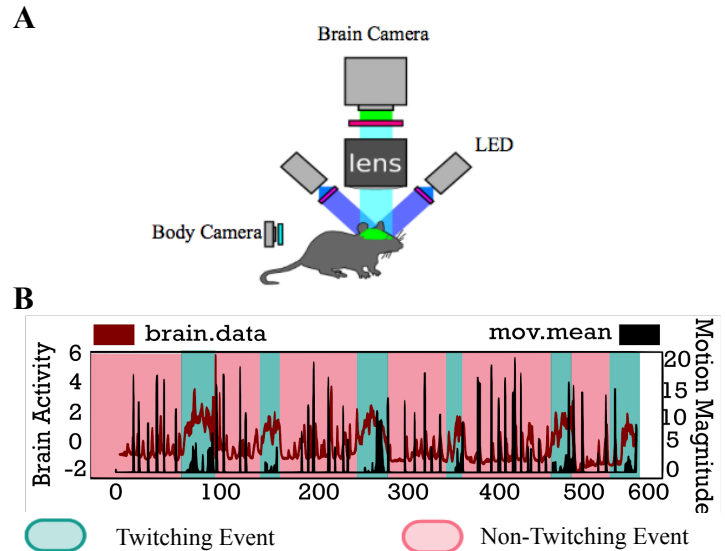
Identifying Behavioral Movements of a Mouse Using Machine Learning

Shreya Mantripragada, Emma Dionne, and Jimmy Chen

Abstract— **In developmental neuroscience, there is a need to understand how state plays an active role in the developing brain. This paper presents a novel approach of using machine learning techniques to distinguish two states in early postnatal mice, twitch and non-twitch occurrences, using information from its gross brain activity and body camera recordings. Supervised machine learning was initially done to help gain insight into associations between human classifications and the training metrics. However, the goal of the work was to come up with an accurate unsupervised machine learning technique [2] that closely represented the results of the human classification. Throughout this process, data reduction and clustering techniques were used to develop this unsupervised machine learning algorithm. Results were then validated against the human classification resulting with an accuracy of 82.6%. These initial results will allow researchers to use our algorithm as a starting point to test machine learning algorithms on other behavioral states occurring in a variety of animals, furthering our understanding of the principal connections between the brain and body.**

I. INTRODUCTION

The human brain controls, monitors, and regulates an individual's bodily functions. To establish proper functions, developmental brain waves help to link the body function to the complex brain structures. These processes of the brain's development from neonate to adult are vaguely understood. It is hypothesized that sleep cycles are necessary for perinatal brain development, a vital stage in which the brain forms and develops proper connections, aiding in memory and brain functionality [1]. Due to the structural and functional similarities between a human brain and a mouse's brain [1], we can begin to look at emergent developmental patterns in perinatal mice. To do this, we recorded from postnatal day 7 mice brain activity, through pan-neuronal expression of a genetically encoded calcium indicator, while recording body movements (Fig. 1A). We identified periods of time when the mouse pup displayed signs of *active-sleep*. During these *active-sleep* periods, mice undergo a series of unconscious movements throughout the body, classified as twitching events. The average brain activity across the neocortex was taken to represent the distinct mental states. The behavioral data was processed using Optic Flow functions that approximate the amount of motion that occurs between two subsequent frames. When we juxtapose the average brain activity with the average motion, we noted the time frames of twitching (small motions with short inter-event time-lag) aligned with high amounts of brain activity (Fig. 1B, blue periods). This direct relationship of twitching events in the mouse's body with high neurological activity is the relationship we sought to explore using machine learning applications.
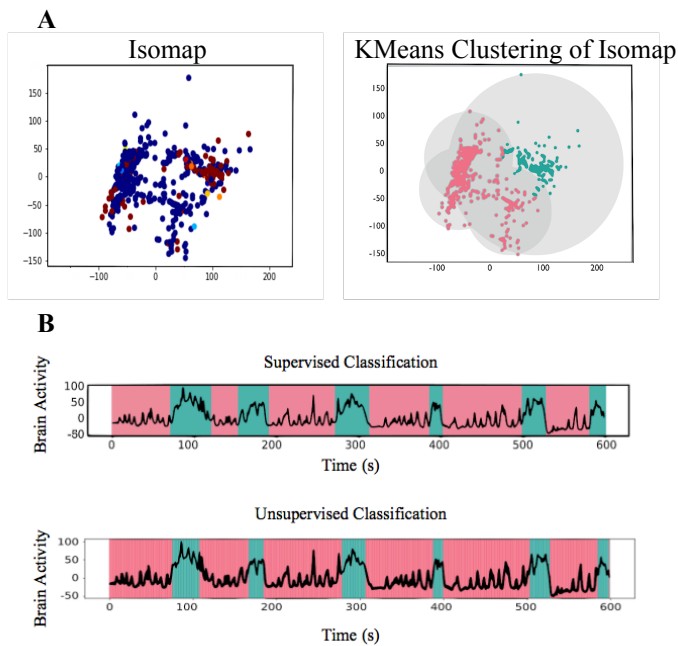

A

B

Figure 1A: *The experimental setup on the mouse in order to receive its body movements and brain activity through cameras that were placed next to the mouse's body and above its brain.*

Figure 1B: *Average brain activity (maroon line) on top of the average movement data (black line) showed the two distinct states of which we call twitch (blue periods) and non-twitch (pink periods).*

II. METHODS

The initial pieces of data were the mouse's neural signals and physical body movements. From these two metrics, the list was expanded to over 30 different features by taking mathematical derivations and operations (ie: derivatives, ranges, windowed standard deviations, etc.) of the initial two metrics. This expanded list of metrics was narrowed down to metrics that allowed for good separation of twitching and non-twitching events, based on human classification. We visualized this separation through pairplot graphs, which plotted each of the metrics against all other metrics. From these pairplots, we selected 4 metrics that best distinguished the two states, and these 4 chosen metrics were then reduced into two dimensions using dimension reduction algorithms such as t-SNE and isomap. Dimensionality reduction creates a new copy of the data and reduces the data-set from 4 to 2 dimensions, allowing us to better visualize the numerical information. Further, we utilized the reduced dimension dataset to cluster our input data to two states. The dimensionality reduction technique that proved to be the best for clustering was KMeans (Fig. 2A). Once those instances were classified, a clean-up algorithm was created for the unsupervised classifications to eliminate the outliers and clearly classify complete twitching events. Due to the

success of the KMeans Clustering Algorithm, the four metrics were plotted over the brain activity and, as shown by Fig. 2B, were successful in classifying the number of twitching movements, as well as their general duration. Due to the similarities between our Unsupervised Machine Learning output to the Supervised Machine Learning result, where the specific time series values of the twitch events were inputted, the four metrics chosen were proven to be successful.

A

Isomap

KMeans Clustering of Isomap

B

Figure 2A: The leftmost figure displays an isomap dimension reduction of all human classified data points, distinguishing twitching (red dots) and non-twitching (blue dots) occurrences. The rightmost figure shows KMeans clustering on the isomap with the unsupervised clustering classification of twitches (light blue) and non-twitches (pink).

Figure 2B: *Comparison between the supervised classification and the unsupervised classification, with twitch periods (light blue) and non-twitch periods (light pink).*

III.   RESULTS

After testing the different dimensionality reduction methods and clustering algorithms on our unsupervised machine learning, isomap dimensionality reduction and KMeans clustering proved to be the best means of classifying the two states, twitch and non-twitch. Even though the unsupervised classifications were not perfect, a quick clean-up algorithm perfected the classifications and captured the distinction between the two states, resulting in an improved final accuracy of 82.6%. In comparison, the supervised learning resulted in an accuracy of 94.0%. While the unsupervised learning underperformed in accuracy, the unsupervised learning had only a 11.4% difference.

IV.   DISCUSSIONS

In this study, we set the goal to develop an unsupervised learning algorithm that could detect two distinct states, twitch vs non-twitch, of a developing neonate mouse based on gross neocortical activity and movement data. Identification of the periods in which there is purported active sleep (twitch state) will help developmental neuroscientists to study the emergence of properly functional networks and highlight the importance of these necessary periods for the developing system. We have successfully demonstrated that an unsupervised machine learning approach can be used to identify these periods. Future researchers can build off of these concepts to better implement machine learning to complicated biological processes, using both neural activity and behavior.

V.   ACKNOWLEDGEMENTS

VI.   REFERENCES

1.   Snyder, J. M., Hagan, C. E., Bolon, B., & Keene, C. D., "Comparative Anatomy and Histology," *PDF*, 2nd ed., 2017, pp. 403-444.
2.   Aurélien Géron, "Hands-On Machine Learning with Scikit-Learn & TensorFlow, " *Paperback*, 1st ed. vol. 1, O'Reilly Media Inc, 2017.

The Healing Effects of Healthy Blood Flow in Kidney and Endothelial Cells Damaged by Coal Nanoparticles

David Lee

Abstract — **Coal is used as a major energy source throughout the world. The production and burning of coal not only harms the environment but also causes serious health problems in those that depend on it. While much research has been done on its respiratory effects, research on other organs is lacking. This study investigates the viability of utilizing healthy blood flow conditions (shear stress), such as an exercise state, to induce cell healing in endothelial cells and inhibit apoptosis in kidney cells. The experiments confirmed that kidney cell damage from coal particles was recovered by exposing cells to shear stress or by treating the damaged cells with secreted substances of endothelial cells exposed to shear stress. Changes in apoptosis-related genes (Bax, FAS, Bcl2l) were also observed in kidney cells after media transplantation. These results illustrate that activities such as exercise to create a healthy blood flow have the potential to treat cell damage caused by coal particles and inhibit renal apoptosis.**

I. INTRODUCTION

While the production of coal in some countries is now declining, many major countries still use coal as a major energy source, and coal still has a major impact on the lives of millions of people around the world. While multiple studies have alluded to a relationship between coal dust inhalation and other non-lung-related diseases, such as kidney disease, research on the topic has been minimal. This study aims to identify potential alternate methods for treating coal-induced kidney and endothelium damage. As recent studies have demonstrated the healing effects of shear stress, or healthy blood flow, in cells (for example, orbital shear stress has been shown to influence expression of the iNOS protein and phosphorylation of Protein kinase B in rats), the viability of using shear stress as a treatment option for damaged cells was tested. Additionally, endothelial cells interact with various organs, including the kidney, through secreted factors in the bloodstream. As these factors have been proven to have significant effects on other organs, the study also tests the viability of using the endothelial cell secretion resulting from coal particles to heal kidney cells.

II. METHODS

Coal samples 1 and 2 were prepared by mixing unburned and burned coal powder samples, respectively, with phosphate-buffered saline (PBS) and filtered using a 0.22 um filter. Samples 3 and 4 were prepared by autoclaving the unburned and burned coal powder samples, respectively, and dissolving each sample to a 10 mg/mL ratio in PBS. Calf pulmonary artery endothelial cells (CPAE) and Madin-Darby Bovine Kidney cells (MDBK) were used in the experiments. After treating cells with the coal samples, the optical density value for each well was read by a UV spectrophotometer to determine the cell viability. Shear stress was applied by using magnetic bar and stirrer machine to simulate healthy blood flow. In order to examine the effects of secreted substances from endothelial cells on kidney cells, coal samples 1 and 2 (samples 3 and 4 were excluded due to their excessive toxicity) were applied to CPAE cells, and the cells were exposed to shear stress (SS) or left static (ST) for 48 hours. The remaining media was then transplanted onto MDBK cells, and cell viability was analyzed. The expression of apoptosis-related genes (Bax, Bcl2L, and FAS) after media transplantation was also analyzed through Reverse Transcription PCR. The data are presented as the mean ± standard error (SE) of at least 3 independent experiments. After intergroup differences were analyzed using a Microsoft Excel statistical function, an F-homogeneity of variance test was conducted, and the t-value of samples were obtained. A p value of < 0.05 was considered statistically significant.
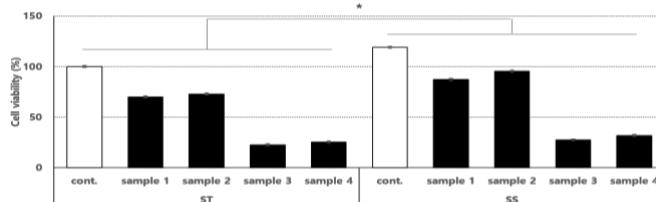
III. RESULTS AND DISCUSSION

Figure 1. *The anti-apoptotic effect of shear stress on endothelial cells treated with coal*
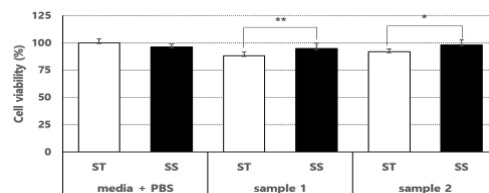

Figure 2. *The anti-apoptotic effect of media from shear stress exposed CPAE cells on MDBK cells*
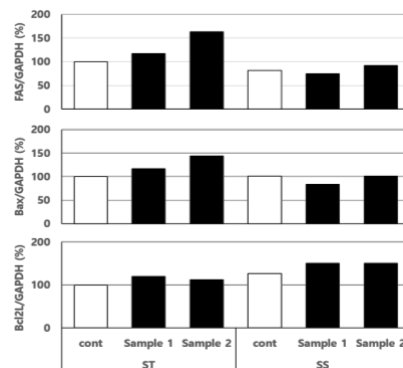
96-Well Plates", *SLAS Discovery: Advancing Life Sciences R&D*, 15(4), 2010.

[6] Thierry Z., Alexander R. W., Nerem R. M., "An Endothelial Cell-Smooth Muscle Cell Co-Culture Model for Use in the Investigation of Flow Effects on Vascular Biology", *Annals of Biomedical Engineering*, 23(3), 1995.

[7] Sumathy M., Natarajan M., Anthony J. V., Eugne A. S., "Regulation of Low Shear Flow-Induced Haec Vcam-1 Expression and Monocyte Adhesion", *American Journal of Physiology-Cell Physiology*, 276(5), 1999.

[8] Maria L. C. A., Christopher M. W., Ushma S., H. William S., Annette S. F., "Shear Stress Enhances Human Endothelial Cell Wound Closure in Vitro", *American Journal of Physiology-Heart and Circulatory Physiology*, 279(1), 2000.

[9] Gyeong I. M., Sue I. J., Yong C. B., "Laminar Shear Stress Induces the Expression of Aquaporin 1 in Endothelial Cells Involved in Wound Healing", *Biochemical and Biophysical Research Communications*, 430(2), 2013.

[10] Nobuyoshi A., S. Aydin D., Masataka I., Hiroyuki K., Nobuyuki A., Tadahiro S., Bauer E. S., "Endothelial Cell Response to Different Mechanical Forces", *Journal of Vascular Surgery*, 32(4), 2000.

[11] Scott M. W., James N. T., "Adaptation of the Endothelium to Fluid Flow: In Vitro Analyses of Gene Expression and in vivo Implications", *Vascular Medicine*, 9(1), 2004.

[12] Alan R. B., Peter I. L., Gabor M. R., "Gene Expression Profiling of Human Aortic Endothelial Cells Exposed to Disturbed Flow and Steady Laminar Flow", *Physiological Genomics*, 9(1), 2002.

Figure 3.   Changes in apoptotic and anti-apoptotic gene expression following CPAE media transplantation

After applying coal samples to endothelial cells, cell viability was noticeably greater in cells that received shear stress compared to cells that were left static in all cases, including the control groups (Fig. 1). This suggests that healthy blood flow can directly reduce the damage that coal particles have on endothelial cells and can potentially aid in the healing process.

When the CPAE cell culture media was transplanted onto MDBK cells, the media from shear stress exposed CPAE cells resulted in a higher cell survival rate in MDBK cells than the static samples (Fig. 2). As shear stress did not change the chemical composition of the coal particles that were in the media, we can conclude that the secreted substances resulting from shear stress application were responsible for the increased viability in the MDBK cells.

Additionally, the media from shear stress exposed CPAE cells caused significant differences in apoptosis-related gene expression in MDBK cells when compared to static samples (Fig. 3). The shear stress sample caused smaller expression levels of the FAS and Bax genes (which induce apoptosis) and greater expression of the Bcl2l gene (which inhibits apoptosis) when compared with static samples. This signifies that the CPAE cell secretion resulting from shear stress has clear anti-apoptotic effects on MDBK cells at the mRNA level.

All experiments demonstrated that the damage caused by coal particles on kidney or endothelial cells can be reduced and repaired by healthy blood flow (shear stress). Future testing of such shear stress application by using in vivo studies is required in order to confirm that the observed results can also be replicated within an entire organism. The confirmation of such results would suggest that generating healthy blood flow through exercise or other means can serve as a simple and cost-effective treatment option to coal-induced damage in the studied organs.

References

[1] Javier C., Suchithra N., Peter D. S., Paul J., "Mortality and morbidity in populations in the vicinity of coal mining: a systematic review", *BMC Public Health*, 18(1), 2018.

[2] Hendryx, M. "Mortality from heart, respiratory, and kidney disease in coal mining areas of Appalachia", *International Archives of Occupational and Environmental Health*, 82(2), 2009.

[3] Hyosoo K., Keun H. Y., Hyunjin C., Geumhee G., Sun C. P., Ji I. K., Sang S. Y., In S. M., "Different Effects of Orbital Shear Stress on Vascular Endothelial Cells: Comparison with the Results of In Vivo Study with Rats", *Vascular Specialist International*, 31(2), 2015.

[4] Jeng-Jiann C., Li-Jing C., Cheng-Nan C., Pei-Ling L., Chih-I L., "A Model for Studying the Effect of Shear Stress on Interactions between Vascular Endothelial Cells and Smooth Muscle Cells", *Journal of Biomechanics*, 37(4), 2004.

[5] Patrick Y. K. Y., Emily P. Y. L., N. K. Mak, Ricky N. S. W., "A Simplified Method for Quantifying Cell Migration/Wound Healing in

Nickel Hydroxide Catalysts with a Large Surface Area for Efficient Water Oxidation: Toward a Hydrogen-Energy Society

Justin J. Choi

Abstract— **Hydrogen is an energy source of the future that can be obtained in an environmentally friendly manner from water splitting. To ensure that hydrogen is generated efficiently using this process, the oxygen evolution reaction (OER) needs to be accelerated to achieve a redox balance. This study intends to develop nickel-based OER catalysts ($Ni(OH)_2$) with large surface areas by employing a surfactant known as P123 in the electrodeposition of catalytic electrodes, and exploits the ability of this surfactant to assemble into micelles and ultimately transform into nanopores. Variation of the P123 concentration indicated that a P123 concentration of 1.6% resulted in the most efficient OER catalytic activity owing to the formation of nanoparticles that embed regular pores. This study conveys an important message, namely that appropriate incorporation of a surfactant in the electrodeposition of a catalytic electrode is a useful strategy to enhance the OER efficiency in the water-splitting process.**

I. INTRODUCTION

Environmental devastation represented by global warming has become a huge concern worldwide. This global issue mainly originates from the use of fossil fuels, and countless trials and attempts to find green energy sources have long been undertaken until it was noticed that the most effective source of energy has always been nearby within plain sight: hydrogen separated from water [1].

Toward this end, electrochemical systems were developed to produce oxygen and hydrogen from water via the oxygen evolution reaction (OER) and hydrogen evolution reaction (HER), respectively. Of these two reactions, driving the OER is more energetically challenging compared to the HER [2]. Therefore, developing efficient OER catalysts takes a high priority in the overall progress toward splitting water. A possible shortcut to achieve this goal would be to increase the surface areas of OER catalytic electrodes, which could be achieved by employing repeated nanometer-scale patterns, such as nanopores. In this respect, it is well known that micelles composed of surfactants can be transformed into regular pores or particles. Thus, in this study, a surfactant was utilized to create regular pores embedded within nanoparticles. By using the highly efficient OER performance of previous nickel-based catalysts as a benchmark [3], nickel hydroxide ($Ni(OH)_2$) was prepared by electrodeposition in the presence of a surfactant named P123 and studied as an OER catalyst. The optimal amount of surfactant that exhibited the highest OER performance was identified, implying a significant step in obtaining hydrogen from an environmentally friendly source: water.

II. METHODS

The electrodeposition of $Ni(OH)_2$ was accomplished by assembling a three-electrode cell containing a precursor solution in which stainless steel foil, Ag/AgCl, and platinum (Pt) wire were used as the working, reference, and counter electrodes, respectively. A constant voltage of −0.5 V or −0.7 V with respect to Ag/AgCl was applied for 20 minutes. Twelve different precursor solutions with different amounts of P123 (0~3.2 wt%) were used for this electrodeposition experiment [4]. Scanning electron microscopy (SEM), transmission electron microscopy (TEM), and small angle X-ray scattering (SAXS) were employed to characterize the morphology of the electrodeposited electrodes. Linear sweep voltammetry (LSV) was used to assess the catalytic activity.

III. RESULTS AND DISCUSSION

Through SEM analysis (Figure 1), it was observed that the nanoparticle formation was more prominent as the P123 concentration increased until 1.6%. However, P123 concentration above 1.6% led to a decrease in the number of particles, which indicates that there exists an optimal P123 concentration (in our case, 1.6%) in $Ni(OH)_2$ nanoparticle formation.
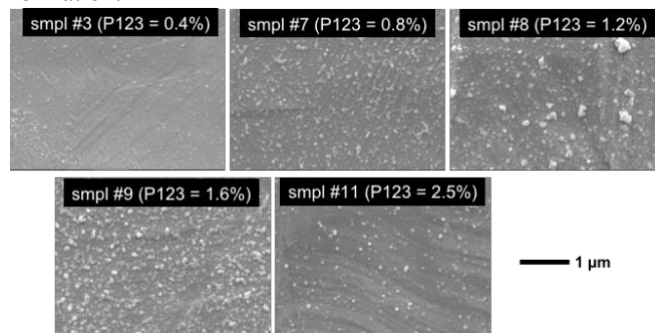

Figure 1. SEM images of $Ni(OH)_2$ electrodes with different amounts of P123 surfactant.

To see if there is the formation of regular pores, SAXS analysis was performed. As shown in Figure 2, as the P123 concentration increased, the intensity of the peak at 1.92° increased until reaching a maximum at 1.6%. Above this concentration, the peak at 1.92° weakened, implying the existence of an optimal concentration of P123 for forming a regular pore pattern. By utilizing Bragg's law, the pore-to-pore distance corresponding to 1.92° was evaluated to be 4.6 nm.
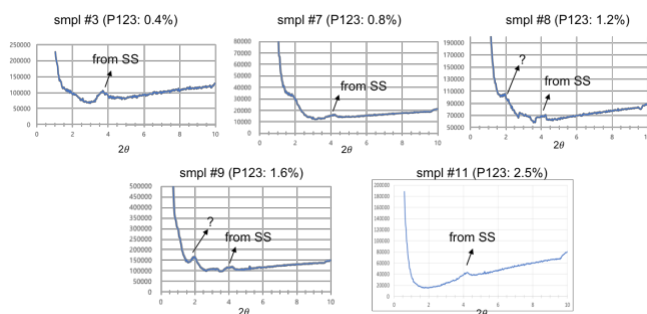
Figure 2. SAXS patterns of Ni(OH)$_2$ electrodes with different amounts of P123 surfactant. SS represents the stainless steel substrate.

In order to confirm that the unknown peak at 1.92° of sample 9 (P123=1.6%) originates from a regular pore pattern, the sample was analyzed by transmission electron microscopy (TEM). Sample 3 (P123=0.4%) was also examined by TEM. As displayed in Figure 3, sample 3 exhibited a lamellar structure consistent with the images in the literature [4]. In contrast, sample 9 was revealed to have a microstructure with repeated contrasts of which the interval is approximately 5 nm. These contrastive dimensions correspond well with the d value of 4.6 nm in the aforementioned SAXS analysis, implying that sample 9 would have a large surface area due to the formation of both nanoparticles and nanopores.
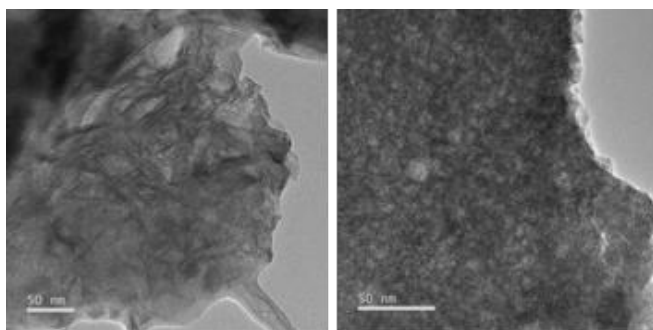

Figure 3. TEM images of samples 3 (left, P123 = 0.4 wt %) and 9 (right, P123 = 1.6%).

The OER profiles of the Ni(OH)$_2$ electrodes were recorded with different concentrations of P123, as shown in Figure 4. All samples displayed the formation of oxygen bubbles once a sufficiently large voltage was applied (photo on the right in Figure 4). Among all the samples that were tested, a P123 concentration of 1.6% exhibited the steepest OER profile, indicating the most efficient catalytic activity, which is consistent with the SEM, TEM, and SAXS results.
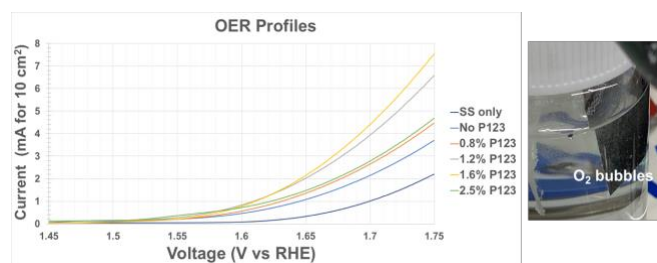

Figure 4. OER profiles of Ni-based catalytic electrodes based on different amounts of P123 surfactant when scanned at 5 mV/s (left). Digital photograph of oxygen bubbles generated from the Ni-based catalytic electrode (right).

IV. CONCLUSION

This study revealed the importance of surface morphology control when designing OER catalytic electrodes. In particular, incorporation of a suitable amount of surfactant can considerably increase the surface area and consequently enhance the OER performance dramatically. Taking advantage of this approach, we foresee the future energy-environment platform illustrated in Figure 5. Drained water from our everyday lives can be collected in an electrolyzer that splits water into hydrogen and oxygen. This hydrogen gas can be used to charge fuel cell vehicles so that our environment can benefit while use of fossil fuel energy is minimized.
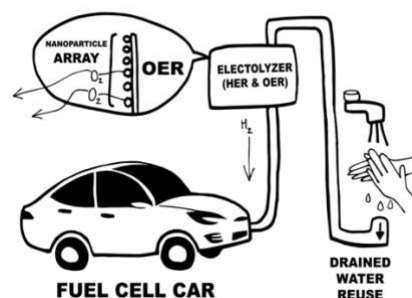

Figure 5. Suggested scheme for reusing drained water for powering fuel cell cars, which are supplied with hydrogen by an electrolyte with efficient HER and OER catalysts.

REFERENCES

[1] M. G. Walter, E. L. Warren, J. R. McKone, S. W. Boettcher, Q. Mi, E. A. Santori, N. S. Lewis, "Solar Water Splitting Cells", *Chem. Rev.,* Vol. 11011, 2010, pp. 6446-6473

[2] Y. Yan, B. Y. Xia, B. Zhao, X. Wang, "A review on noble-metal-free bifunctional heterogeneous catalysts for overall electrochemical water splitting", *J. Mater. Chem. A*, Vol. 4, 2016, pp. 17587-17603

[3] L. Chen, X. Dong, Y. Wang, Y. Xia, "Separating hydrogen and oxygen evolution in alkaline water electrolysis using nickel hydroxide", *Nature Commun.*, Vol. 7, 2015, 11741

[4] Y. Tan, S. Srinivasan, K.-S. Choi, "Electrochemical Deposition of Mesoporous Nickel Hydroxide Films from Dilute Surfactant Solutions", *J. Am. Chem. Soc.*, Vol. 127, 2005, pp. 3596-3604

The Effect of Parenting Style and Personality Type on Classical Musicians' Career Development

Alexis Francis

Abstract— **Classically trained musicians devote the majority of their early lives toward cultivating their expertise and skill. However, it is common to forego a career as a performing artist despite years devoted to musical study. This quantitative study surveyed classically trained musicians to assess how the parenting style in which they were raised and how their personality traits affected their satisfaction with their overall career choice. Besides performance, occupations of surveyed participants included teaching music and careers outside of music performance and teaching. Musicians who were performing musicians, as well as those who were in careers related to music, were most satisfied whereas those who ended up pursuing careers not related to music were less satisfied. The majority had parents who were high in both Demandingness and Responsiveness; however, parenting style did not show a statistically significant trend relative to whether or not musicians ended up in performance careers nor did it influence whether or not they were satisfied with their career choice. Of note were the high levels of Neuroticism seen in many participants, suggesting the choice to pursue an occupation as a performing musician may be a difficult path for many people. A deeper look at the outcomes related to the intense study of classical music is warranted to assess if it is indeed the right choice for the student.**

I. INTRODUCTION

Parental support and influence play an important role in the development of classically trained musicians given they commence playing at such a young age and devote years to study music. However, no research to date has examined how parenting style affects their long term career satisfaction.

II. METHOD

In the present study, personality traits of classically trained musicians (measured by the Big 5 FFM) and the parenting styles (assessed by the PSI-II) with which they grew up were captured via a survey. The relationship between these characteristics and musicians' career satisfaction was analyzed. Participation in the current study was voluntary, and the participants understood the nature of the study and consented to participate.

III. PARTICIPANTS

Participants were 41 adults who received their training and degree from prestigious conservatories. Participants ranged in age from 30 to 45 with an average age of 37.4. The breakdown in sex was 53.7% female and 46.3% male. A majority was Caucasian (63.4%). The others were Asian (29.3%), Hispanic (2.4%) and other ethnicities (4.9%). The highest level of education attained by participants included Doctoral degree (43.9%), Master's degree (39%), Professional studies degree (7.3%), Artistic diploma (7.3%), and Bachelor's degree (2.4%). Most participants majored in piano (24.4%), voice (22%), or composition (29.3%). Participants started music lessons at a young age with 39% starting between 3 to 5 years old, 29.3% starting between 6 to 8 years old, 9.8% starting between 9 to 10 years old, and 12.2% starting between 11 to 13 years old. More attended pre-college (51.2%) than not (48.8%). Participants had careers in teaching (43.9%) and performance (36.6%) with 19.5% responding they had careers outside of these two areas.

IV. EXPERIMENTAL DESIGN

In order to assess the musicians' personality traits, the NEO Five-Factor Inventory-3 report was used to assess respondents' Big 5 FFM. It is a 60-item questionnaire that provides a quick, reliable, and accurate measure of the five domains of personality (Neuroticism, Extraversion, Openness, Agreeableness, and Conscientiousness) and has been used to determine personality traits in previous studies (Vedel 2016). Capturing musicians' personalities was deemed useful to assess if children with varied personality traits may react differently to certain parenting styles.

A literature search was conducted to look at past studies that assess personality and childhood upbringing based on the children's perspectives. The Parenting Style Inventory-II (PSI-II) is a 15-item self-report measure of parenting style based on children's attitudes and general experiences with their parents (Chen 2015). The 15 items are divided equally into three subscales, which represent three dimensions of parenting: Responsiveness, Autonomy Granting, and Demandingness. Surveys were emailed to participants in two parts: 1) the Survey (Qualtrics) which included the PSI-II questions and 2) the NEO-FFI-3 online assessment.

On average, participants spent approximately 10 minutes completing the survey (5 minutes for Qualtrics and 5 minutes for PSI-II) and approximately 10 minutes on the NEO-FFI-3 assessment.

V. MEASUREMENTS & CALCULATIONS

The results of personality types and parenting styles among participants are shown in Table 1 and Table 2.

TABLE 1

Classical Musicians' Personality Traits Ranges					
Level	*Neuro-ticism*	*Extra-version*	*Open-ness*	*Agree-ableness*	*Conscien-tiousness*
Very High	9	0	15	1	2
High	14	6	15	9	15
Average	14	22	5	16	13
Low	3	11	6	12	11
Very Low	1	2	0	3	0

Numbers represent participants who fall within each range.
Very High (≥66), High (56 to 65), Average (45-55), Low (35-44), Very low (≤34)

TABLE 2

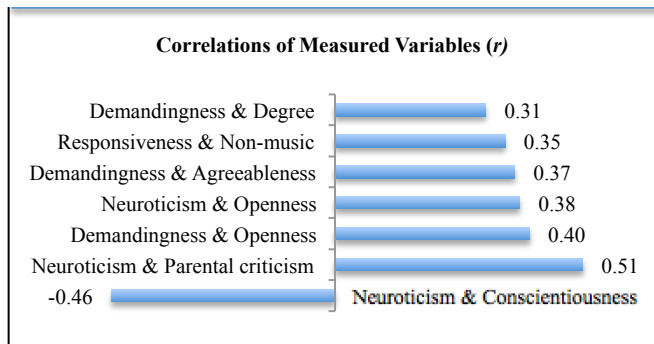| Parenting Style (PSI-II Results)			
Level	Responsiveness	Autonomy Granting	Demandingness
1 to 10	2	3	0
11 to 19	17	25	24
20 to 25	22	13	17

Numbers represent participants who fall within each range.

V. Data Analysis

The highest satisfaction career groups (highest score being 5) were performing musicians, namely, orchestra and choir members and those musicians whose work related to music production (mean satisfaction score for both = 4)

A bivariate correlation analysis was conducted to determine if there were correlations between various metrics. Those in Table 3 below were found to be statistically significant.

TABLE 3

Correlations of Measured Variables (r)

Demandingness & Degree — 0.31
Responsiveness & Non-music — 0.35
Demandingness & Agreeableness — 0.37
Neuroticism & Openness — 0.38
Demandingness & Openness — 0.40
Neuroticism & Parental criticism — 0.51
Neuroticism & Conscientiousness — -0.46

$p \leq 0.05$, Correlations on other variables did not yield statistically significant results.

TABLE 4

Parenting Styles and Resulting Careers			
Style	Performance	Teaching	Other
High Demandingness/ High Responsiveness	9	12	7
High Demandingness/ Low Responsiveness	3	1	0

Numbers represent participants who fall within each range.

VI. Discussion

The results of this study did not show a statistically significant trend between parenting style and musicians' resulting career. One issue encountered in the study was the small sample size. Of the 41 musicians who participated in the study, only 4 had parents who were both high in Demandingness and low in Responsiveness. Although three of these musicians work in performance, there were no consistencies among their personalities compared to the one participant who did not. Twenty-eight participants had parents who were both high in Demandingness and Responsiveness, but their personalities and resulting careers had no statistically significant correlations.

There were, however, statistically significant relationships to note among personality traits and parenting characteristics. In particular, Demandingness in parents strongly correlated with Openness and Agreeable personality traits in musicians. This suggests that parents with high

levels of Demandingness strongly encourage their children to achieve what the parents deem important; children who are agreeable and open are likely to comply with their parents' wishes. As such, children may be pushed to start music lessons young, start precollege young, achieve higher degrees in music, etc. Although in many situations, having parents high in both Demandingness and Responsiveness is more likely to lead to successful outcomes (Chen 2015), this was not the case for people who want to become classically trained performing musicians since the results of being satisfied with career choice were mixed in this group of participants.

In addition, parents with high Demandingness levels also strongly correlated with high levels of musician Neuroticism. High levels of Neuroticism in individuals have been shown to cause moodiness and negative feelings such as anxiety and depression. The findings of high levels of Neuroticism in the participants of this survey echo a recent finding that suggested musicians could be up to three times more likely to suffer from depression compared to the general public (Gross 2016). Therefore, although demanding parents may be successful at pushing their children toward high levels of musical accomplishment, this goal may come with downsides.

There were trends in the study that suggested responsive parents were more likely to have children who choose their own path upon finishing conservancy. Many quit music and pursued other careers. Despite working in careers other than music performance, these children still showed high levels of career satisfaction, similar to that of performing musicians. This suggests parents with high Responsiveness supported their children's decisions regardless of career choice and these musicians were satisfied regardless of the level of achievement they attained in music performance.

The right parenting styles for children who wish to pursue classical music is debatable based on these study results. It appears there are some advantages to having parents with high Demandingness, as it relates to musicians achieving high levels of music accomplishment; however, it may negatively affect the child's overall wellbeing. Further research is warranted to look at the effects of parenting style on classically trained musicians to determine the effects on their overall satisfaction with their career choice.

References

[1] Chen, W. (2015). Relationships between perceived parenting behaviors and academic achievement among high school students in the International Baccalaureate (IB) programs: A comparison of Asian American and White students. Doctoral dissertation, University of South Florida. ProQuest Dissertations and Theses Global.

[2] Gross, S.A. and Musgrave, G. (2016). Can music make you sick? Music and depression: A study into the incidence of musicians' mental health. Academic study, University of Westminster/Music Tank.

[3] Vedel, A. (2016). Big five personality group differences across academic majors: a systematic review. *Personality and Individual Differences, 92*, 1-10.

Modeling Uranium Uptake in Fossilized Teeth and Bones: Potential for Long-Term Uranium Waste Storage

Ethan Sontarp, E. Troy Rasbury, William Holt, and Kathleen Wooton

Abstract—**The purpose of this study is to quantitatively model the uptake of uranium (U) in porous biomaterials, such as a fossil tooth and bone. An understanding of the systematics of U uptake in phosphates has the potential to optimize the materials used in the field of nuclear waste remediation. Laser Ablation Inductively Coupled Plasma Mass Spectrometry (LA-ICP-MS) was utilized to determine the uranium/lead isotopic ratios for biomaterials in the fossils, which then informed the creation of a MATLAB model based upon the exponential falloff rate equation, designed to match the experimental data. Conjugate gradient technique solved for the best-fit e-folding time for the rate of uptake, with the e-folding time for the bone sample being 1.3 Ma, and the tooth 0.9 Ma, respectively. Porous phosphates are worthy materials for the remediation of high concentrations of U waste and are able to hold U for millions of years.**

I. Introduction

Nuclear meltdowns and waste mishandling have left some of the groundwater supply contaminated with uranium (U), and efforts to combat this have resulted in studies about nuclear waste remediation which are relatively short in terms of the geologic time scale [1]. The process by which U is taken up and stored in a porous material is integral to the study of nuclear waste remediation. In the form of the uranyl ion, $(UO_2)_{2+}$, U can be immobilized by the phosphates present in mammal teeth and bones. The potential for phosphates to be used as effective remediators remains a promising and cost-effective alternative to the nuclear waste containers being evaluated by the Yucca Mountain Site Characterization Project [2].

The Barstow Formation of Southern California contains an abundance of preserved fossils. Two fossils, a tooth and a foot bone of the ancient horse species *Scaphohippus intermontanus,* were included in this study. They were found at Robbins Quarry, in the Barstow Formation's Hell Gate Basin, which is radiometrically dated at 13.86 ± 0.65 Ma [3]. Each sample underwent diagenesis shortly after burial, taking up high concentrations of U in the process.

II. Methods

Samples were first placed into an epoxy to preserve their fragile structures, then cut into 5-millimeter-thick cross-sections and polished. In order to find the concentrations of U and its daughter product lead (Pb) in the samples, 160-micron diameter spots were ablated in selected areas of the tooth and bone samples using an Agilent 7700 Series Laser Ablation Inductively Coupled Plasma Mass Spectrometer (LA-ICP-MS). Two standards, NIST-612 glass and Walnut Canyon carbonate, were ablated alongside the samples to ensure accuracy in the laser measurements [4-5]. The LA-ICP-MS data were imported into the Iolite software of the Igor Pro program, where the Geochron-4 Data Reduction Scheme was employed to convert the measurements into U and Pb concentrations for each ablated spot. Several hypothetical patterns of U uptake, including a decreasing linear rate of uptake, exponential falloff rate of uptake, and multiple periods U uptake, were then explored for their confirmation to the U and Pb concentration data.

III. Data Analysis

A MATLAB code was designed to read in data collected from individual LA-ICP-MS ablations, and then model the uptake of U in the materials accordingly. The model assumes an exponential falloff rate because it provided the best match to the LA-ICP-MS data, with high concentrations of U being continually taken up over the period of burial. The initial concentration of U in the samples must have been negligible at the time of the animals' deaths, and then would have been rapidly taken up during burial to have led to the state of diagenesis in the samples. Following the initial diagenesis, the rate of U uptake must have slowed due to the decrease in pore space accompanying any precipitation of uranium where there was formerly organic matter.

The code calculates the τ value, a time constant representing the e-folding time for U uptake rate, indicating the timescale in which the majority of the U was taken up in each sample. The best-fitting τ will serve as a match between the experimental data and exponential falloff model.
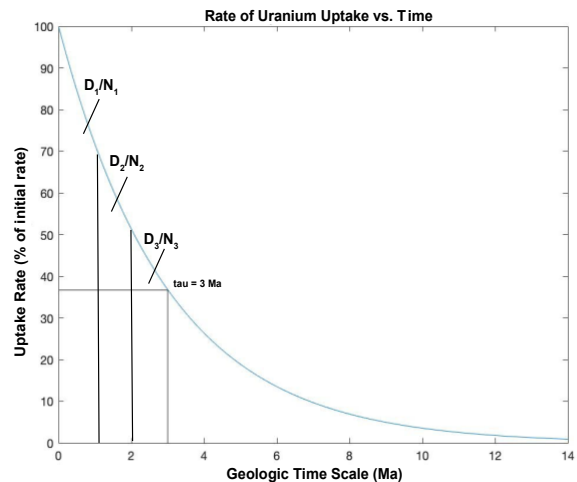

Figure 1. Rate of uranium uptake over a timescale of 14 million years, or the age of the Barstow samples. When the τ is set at 3 Ma, the rate of uptake is given by the initial concentration of uranium over e. D is defined as the number of daughter atoms (Pb) and N the number of parent atoms (U).

IV. Results and Discussion

The τ value indicates the manner of U uptake in a sample, with a large τ symbolizing a prolonged period of uptake and a small τ specifying rapid initial uptake with a quick falloff. Isotopic information from seventy-one spots in the spongy bone region of the fossilized horse bone was used to produce a best fitting τ value, which occurred at 1.3 Ma after the bone's burial. This τ value was then used to predict the age of burial of the sample, producing an age of about 14 Ma, which is consistent with the radiometric age of Robbins Quarry from which the samples were sourced, seen in Fig. 2 below.
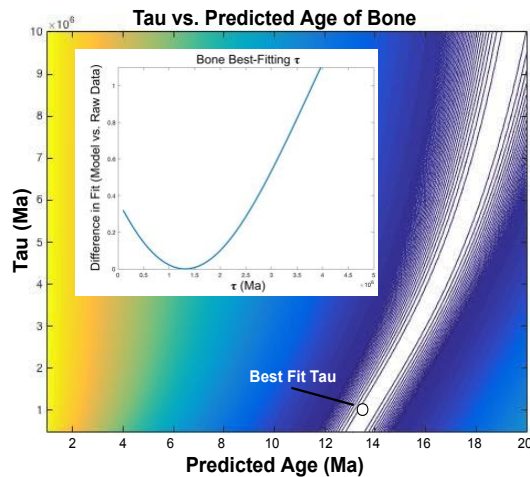

Figure 2.   Best-fitting τ value for the bone sample and its relation to the predicted age of the sample.

This indicates that the bone sample underwent rapid diagenesis resulting in its preservation and the inclusion of thousands of parts-per-million of U atoms into its phosphate structure. 1.3 Ma after the burial of the animal, the rate of uptake had decreased by a factor of e. In addition, the τ value provides insight into the systematics of U uptake with respect to burial age, with a tradeoff taking place between the τ value and the burial age. This confirms that the model is effective for predicting the systematics of U uptake in a preserved fossil bone and demonstrates this biomaterial's ability to sequester U over a timescale of 14 Ma. If a material similar to this porous phosphate were used to remediate nuclear waste, it would remain effective over a timescale of millions of years.

The model was again used to predict the τ value for the ablated localities in the fossilized tooth. After 0.9 Ma, the rate of U uptake in the fossilized tooth slowed by a factor of e. Furthermore, the model again predicts the correct age of burial of the sample, 14 Ma. This confirms that the model is effective for predicting the systematics of U uptake in a preserved fossil tooth and demonstrates the tooth's ability to sequester U over a timescale of 14 Ma.

In comparison with the bone sample, the tooth sample took up its U at a slightly more rapid rate, with the e-folding time being 0.9 Ma, and the bone's e-folding time being 1.3 Ma. The tooth's less rigid structure has contributed to its ability to continually take up U. The dentine and spongy bone biomaterials have the ability to absorb large quantities of U in a short period of time and would effectively sequester U waste for millions of years.
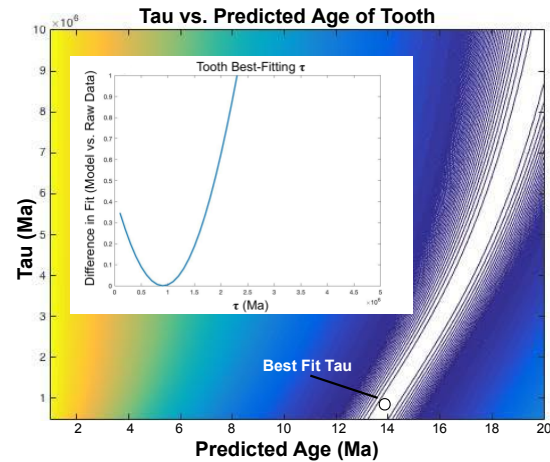

Figure 3.   Best-fitting τ value for the tooth sample and its relation to the predicted age of the sample.

V. Conclusions

By taking advantage of preserved geologic samples, a history of U uptake was determined for a 14-million-year-old *Scaphohippus intermontanus* horse tooth and foot bone, predicting the timeline of radioactive waste immobilization. Both uptake histories describe the ability of porous phosphates to retain high concentrations of U for long periods of time. Impressively, the experimental samples have undergone the highly active tectonic history of Southern California over the last 14 Ma and serve as great examples of the phosphate retention of U matter during fluid flow events. In contrast to the high costs of operating an external waste treatment site, a material which is similar to the porous phosphates could be used as an effective and cheap remediator if injected into an in-situ waste immobilization system, such as a Permeable Reactive Barrier.

References

[1] Crowley, K. D. (1997). Nuclear waste disposal: the technical challenges. *Physics Today*, *50*(6), 32-39.

[2] Gdowski, G. E. (1997). *Degradation mode survey candidate titanium-base alloys for Yucca Mountain project waste package materials. Revision 1* (No. UCRL-ID-121191-Rev. 1). Lawrence Livermore National Lab., CA (United States).

[3] Woodburne, M. O., Tedford, R. H., & SWISHER III, C. C. (1990). Lithostratigraphy, biostratigraphy, and geochronology of the Barstow Formation, Mojave Desert, southern California. *Geological Society of America Bulletin*, *102*(4), 459-477.

[4] Hollocher, K., & Ruiz, J. (1995). Major and trace element determinations on NIST glass standard reference materials 611, 612, 614 and 1834 by inductively coupled plasma-mass spectrometry. *Geostandards Newsletter*, *19*(1), 27-34.

[5] Roberts, N. M., Rasbury, E. T., Parrish, R. R., Smith, C. J., Horstwood, M. S., & Condon, D. J. (2017). A calcite reference material for LA-ICP-MS U-Pb geochronology. *Geochemistry, Geophysics, Geosystems*, *18*(7), 2807-2814.

Detection of Pyridine and BTEX Solvents in Aqueous Media via a Novel Luminescent Metal-Inorganic Framework

Jehil Mehta

Abstract— Benzene, toluene, ethylbenzene, and xylene (BTEX) are harmful chemicals that are found in post-fracturing water which could eventually contaminate ground and surface water. Hydraulic fracturing is a process that is necessary to extract natural gas and oil for industrial purposes as they account for about 80% of energy consumption in the United States. A novel metal inorganic framework (mFMIF), an isomorph of the previously known FMIF-1(fluorous metal-inorganic framework) , has shown to be effective in detecting the previously mentioned carcinogens. mFMIF is a hydrophobic luminescent powder that maintains a blue-green emission when excited by 356 nm light even when completely submerged in water for an extended period of time. When mFMIF is exposed to certain hydrocarbons dissolved in water, such as benzene, toluene, xylenes, and dichloromethane, it results in a bathochromic shift in the emission of mFMIF. Currently, these contaminants are largely identified through either gas chromatography with mass spectroscopy (GC-MS) or gas chromatography with electrolytic conductivity detection (GC-ELCD). Since changes in emission were observed to determine the presence of organic contaminants, the material other benign substances being in water such as slight pH shifts and salinity. mFMIF can be used as an in situ qualitative sensor for organic pollutants in aqueous media as it does not require a trained technician at remote laboratory to test for the contaminants. These contaminants can be tested for by using an inexpensive UV light to test a sample in a vial.

I. INTRODUCTION

Hydrogen and natural gas utilization as an alternative to more-carbon-rich fuels is of immense importance toward energy technologies. While the U.S.'s recent rise as the world's largest producer of natural gas, which can enable a 50% reduction in carbon emissions vs gasoline, instill greater confidence in our energy future, significant challenges remain that stem from the economic and environmental impacts resulting from the millions of gallons of water that are necessary and becoming dangerously contaminated daily due to induced hydraulic fracturing (i.e., "fracking") processes. US Environmental Protection Agency (EPA) studies have shown that the water harms water supplies and can lead to diseases among workers and residents living near these fracking sites. Current detection processes are too time consuming and expensive and lax regulations do not incentivize companies to undergo detection tests. mFMIF provides a method for companies to detect potential contaminants rapidly without having to send samples to a remote laboratory for testing. mFMIF is a powder that can be used on site to test for contaminants with the presence of a luminescence change that can be seen with an ultraviolet light.

II. METHODS

mFMIF was used to test how effective it was at detecting the presence of prominent toxic chemicals found in produced water from hydraulic fracturing processes. Synthesis of mFMIF involves synthesizing FMIF-1 using a triazole salt, methanol, and silver nitrate [1]. I prepared 6 vials of mFMIF by dissolving 20 milligrams of previously prepared FMIF-1 in 10 mL of methanol and then rotary evaporated them at 30° C at a speed setting of 7. The mFMIF was then activated at 190° C for 60 minutes as results showed that it was the optimal time and temperature for creating mFMIF with optimal luminescence.6 solutions of water were prepared, contaminated either by benzene, DCM, toluene, xylenes, or pyridine (all solutions were saturated by mixing 10 mL of water with 0.1 mL of the organic compound and stirred at room temperature overnight). Photoluminescence studies on the mFMIF was collected before exposure to the organic compounds and after to observe a difference in the luminescence. I used a syringe to extract 5 mL of only water and transferred it into the mFMIF vial. The solution was placed in a dark environment for 18 hours as 18 hours was an optimal time for FMIF-1 to significantly purify contaminants from water. The solutions were then decanted and allowed to air dry for three days with open top in a safety hood. The samples were then allowed to sit with a closed top for two more days while being protected from light. Six samples were created in which mFMIF (same concentrations as above) was either exposed to a plain water solution, air, aqueous benzene solution, aqueous ethyl benzene solution, aqueous toluene solution, or aqueous xylenes solution. UV-visual spectroscopy was used to observe the fluorescence quenching over a period of 270 minutes.
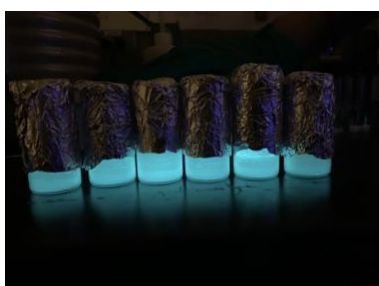
III. RESULTS AND DISCUSSION
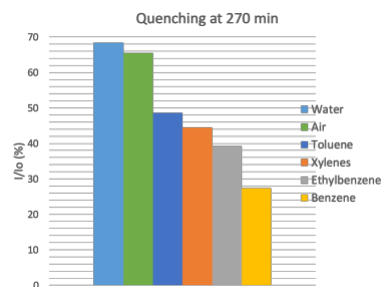
Figure 1: Comparison of the luminescence of mFMIF when exposed to different contaminants during a UV-vis study. Significant decrease in luminescence is depicted when exposed to BTEX.
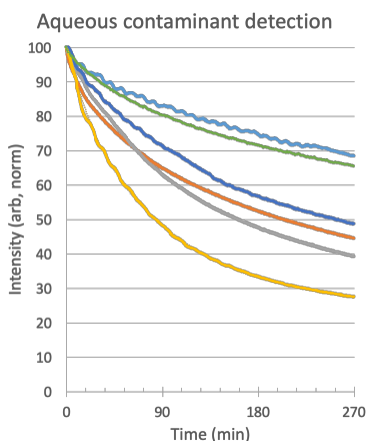
Figure 2: Time based graph of the study showing the decrease of luminescence of mFMIF when exposed to different contaminants.

Figure 3: Samples of unexposed mFMIF
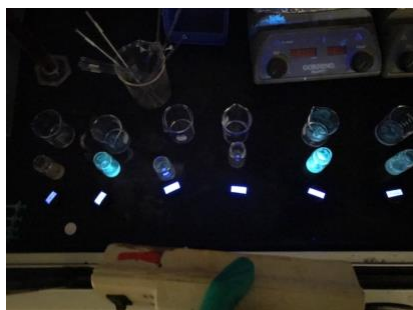
Figure 4: Pictures of samples after exposure to chemicals for 18 hours. From left to right: benzene, dichloromethane, pyridine, toluene, water (control), xylenes.

The need for simple, same day water quality tests is an important requirement that mFMIF may one day fill. It shows comparatively mild quenching for pyridine, toluene, ethylbenzene, and xylenes, along with near complete quenching for benzene. The hypsochromic shift observed with pyridine also provides great promise that mFMIF could be used to identify a variety of contaminants, especially other nitrogen containing aromatics.

A fluorometer was used to conduct photoluminescence studies and different variables were used to determine the conditions for mFMIFs optimal luminescence. I determined that that ideal conditions were using 20 milligrams of FMIF-1 and recrystallizing it in 10 mL of methanol. The optimal heat treatment was determined to be 190° C at 60 minutes.

After exposing six samples of prepared mFMIF to benzene, toluene, ethylbenzene, xylenes, pyridine, and dichloromethane, it was determined that the mFMIF was able to exhibit a significant change in luminescence when exposed to most of the chemicals, with the exception of dichloromethane. Although the control sample also showed a decrease in luminescence, the amount of quenching was minimal when compared to other chemicals that were tested. The intensity of the graphs shows a clear decrease in the luminescence after each sample was exposed to the respective chemicals in comparison to the photoluminescence data before it was exposed to any toxic chemicals. The benzene sample showed the greatest decrease as it lost about 70% of its luminescence after exposure for 270 minutes. The ethylbenzene sample lost approximately 60%, the xylenes sample lost about 55%, and the toluene sample lost about 50%. The air and water sample each lost about 30% of their luminescence, but the difference were negligible and the loss was likely due to photobleaching. The mFMIF sensor that we have been working with has the potential to be commercialized for large scale testing. Further studies can involve acquiring the Stern-Volmer equation that is specific to the mFMIF The formula related variables such as the intensity of the fluorescence when exposed to a quencher (I_f), intensity when not exposed to a quencher (I_{0f}), the rate of quenching (k_q), lifetime of the emissive excited state of the material without a quencher present, and concentration of the quencher ($[Q]$). This equation will also help us use mFMIF for detection in mixed solutions of contaminants.

$$\frac{I_f^0}{I_f} = 1 + k_q\tau_0 \cdot [Q]$$

Figure 5: Stern-Volmer Equation

IV. ACKNOWLEDGMENT

V. REFERENCES

[1] Moghadam, P. Z.; Ivy, J. F.; Arvapally, R. K.; dos Santos, A. M.; Pearson, J. C.; Zhang, L.; Tyllianakis, E.; Ghosh, P.; Oswald, I. W. H.; Kaipa, U.; Wang, X.; Wilson, A. K.; Snurr, R. Q.; Omary, M. A. "Adsorption and Molecular Siting of CO, Water, and Other Gases in the 2 Superhydrophobic, Flexible Pores of FMOF-1 from Experiment and Simulation", *Chem. Sci.* 2017, *8*, 3989–4000. *HIGHLIGHTED BY JOURNAL ON TWITTER.*
[2] Yang, C.; Kaipa, U.; Zhang Mather, Q.; Wang, X.; Nesterov, V.; Venero, A. F.; Omary, M. A. "Fluorous Metal Organic Frameworks as Superhydrophobic Adsorbents for Oil Spill Cleanup and Hydrocarbons Storage", *J. Am. Chem. Soc.* 2011*, 133*, 18094-18097.
[3] Yang, C.; Wang, X.; Omary, M. A. "Fluorous Metal–Organic Frameworks for High–Density Gas Adsorption", *J. Am. Chem. Soc.* 2007, *129*, 15454-15455. *(238 citations as of July 8, 2017)*

The effects of different aquatic environments on the rate of HDPE and LDPE degradation by *Bacillus subtilis*

Aditya Tadimeti

Abstract - The proliferation of plastics in consumer products is resulting in the release of millions of tons of plastic waste into oceans and harming marine ecosystems [1]. Due to their chemical composition, plastics take hundreds of years to decompose [2]. Current methods of handling plastic waste – recycling, landfills and incineration – are proving to be inadequate, harmful, or ineffective. Scientists have discovered that some bacteria can degrade and assimilate polyethylene [3]. *Bacillus subtilis,* – a rod shaped, gram-positive bacterium found in the upper layers of soil – has been shown to degrade polyethylene in above ground locations [4]. This experiment studied the ability of *B. subtilis* to degrade High-Density Polyethylene (HDPE) and Low-Density Polyethylene (LDPE) in aquatic environments of varying salinity to test its viability in tackling plastic pollution in oceans and other water bodies. Degradation was found in all samples and was the highest in freshwater and lowest in ocean water. The results support the hypothesis that *B. subtilis* can potentially be used to help degrade plastic in aquatic environments.

INTRODUCTION

Bacteria, fungi, and viruses produce microbial compounds called lipopeptides which have surfactant properties due to their amphipathic molecular structure. Surfactants lower the surface tension/energy in a medium and oxidize polymer molecules, break down carbonyl groups, and convert them into unsaturated hydrocarbons. Through this 'depolymerization' process, the enzymes break large polymer chains into smaller, water soluble fragments that can pass through cellular membranes, where they get biodegraded within the microbial cells to be used as energy sources [5]. Surfactin, produced by *B. subtilis,* is a very powerful surfactant. *B. subtilis* has been found in oceans and can thrive in a range of conditions. It has a high capacity to secrete proteins which makes it an excellent candidate to study for this application [6]. However, several studies show that salinity reduces microbial activity which could impede biodegradation [7]. If there is reasonable degradation in spite of salinity, deploying this method at scale can be explored as a viable environmentally friendly method for tackling plastic waste in oceans.

METHODS

Step 1: Culturing the bacteria

B. subtilis was obtained in a sterile, 20 x 150 mm test tube, approximately one-third filled with agar. The test tube was left in the lab at room temperature for a day for the bacteria to culture, and it was later placed in a refrigerator to preserve the contents and inhibit growth.

Step 2: Test Tube Setup

36 strips of HDPE of the same size, shape and mass (roughly 17 mg) were each placed in a separate test tube. Bacteria were added to 24 of these test tubes and the remaining 12 without the bacteria were labeled as controls. Both sets of test tubes were then split into 3 equal groups labeled freshwater, ocean water, and brackish water. This process was repeated with LDPE sheets.

Step 3: Water Setup/Incu-shaker

Sterilized water was first added to each test tube. A premade powder called "Instant Ocean" was added to the 'ocean water' test tubes to achieve a salt concentration of roughly 35 parts per thousand to mimic the average salinity of oceans and to the 'brackish water' test tubes to achieve a lower salt concentration of roughly 15 parts per thousand. A salt medium (NaNO3 (2g), MgSO4 (0.5g), KCl (0.5g), Fe2 (SO4)3 (0.01g), KH2PO4 (0.14g), K2HPO4 (1.2g), Yeast extract (0.02g), water 1L) of very low concentration was added to all test tubes to support the bacteria's growth, a process adapted from the work of Vimala et. al [4]. After each tube contained all the necessary elements, they were placed in a rack inside a shaking incubator set at 35°C, the bacteria's incubating temperature.

Step 4: Massing

After 30 days, each polyethylene piece was removed with tweezers and cleaned of bacteria and salt using a 0.1M HCl wash and water. To test whether the 0.1M HCL wash and water caused any degradation of the plastic, additional LDPE and HDPE pieces of shape, size, and mass similar to the test tube samples were weighed before and after a HCl wash; no significant amount of mass degradation was observed. Each piece was laid on a paper towel and heated to around 40-50°C to remove water droplets. No significant polyethylene degradation occurred during the heating (verified by a separate, dry, control). Then, each piece was laid on top of a balance, and its mass was recorded in a data table. The data was analyzed utilizing the statistical and graphing functions of Excel.

MEASUREMENTS/CALCULATIONS

Freshwater

% Degradation	N	Mean	Standard Deviation	SE Mean	95% CI
HDPE	8	5.79%	3.84%	1.36%	(2.59%, 9.00%)
LDPE	8	5.78%	2.20%	0.78%	(3.95%, 7.62%)

Brackish Water

% Degradation	N	Mean	Standard Deviation	SE Mean	95% CI
HDPE	8	5.08%	2.97%	1.05%	(2.59%, 7.56%)
LDPE	8	5.30%	2.04%	0.72%	(3.60%, 7.01%)

Ocean Water

% Degradation	N	Mean	Standard Deviation	SE Mean	95% CI
HDPE	8	3.61%	2.02%	0.71%	(1.92%, 5.30%)
LDPE	8	2.48%	1.26%	0.44%	(1.43%, 3.53%)

DISCUSSION

The degradation as measured by the reduction in mass of the HDPE and LDPE strips was found to be the highest in freshwater and the lowest in ocean water. This supported the hypothesis that *B. subtilis* can degrade polyethylene in saltwater and that degradation is inversely proportional to salinity. Repeating the experiment and comparing results can help establish their validity. Testing some of the test tubes at intermediate points in time can reveal changes in rates of degradation over time.

Research shows that salinity reduces microbial biomass because osmotic stress results in drying and lysis of cells [7]. It is unclear from these results whether the reduced degradation is due entirely to the slower growth of bacteria – resulting in lower Surfactin production – or if Surfactin's effectiveness is also reduced in saline water.

Further research is required to establish *B. subtilis* as a practical option for tackling plastic pollution in oceans. The optimal conditions for high Surfactin production by *B. subtilis* in the laboratory are a slightly acidic initial pH (6.5–6.8) and an incubation temperature of 30°C [8]. Ocean temperatures vary from 2_oC to 35_oC, which is within the range for *B. subtilis* to thrive. However, oceans are typically less acidic with an average pH of 8.1 [9]. This points to the need to find ways to create optimal conditions in the ocean to enhance the production and/or effectiveness of Surfactin.

The superior degradation in freshwater supports the possibility that microbial biodegradation can tackle plastic pollution in freshwater bodies, potentially inhibiting the downstream spread of plastic into oceans. The degradation in brackish water suggests that this method can be used in estuaries and at the mouths of rivers.

Research has shown that pretreatment of polymer films with UV radiation aids its accessibility as food for the microorganisms, enabling a faster rate of biodegradation. This suggests that UV radiation from the sun can aid biodegradation by *B. subtilis* in the ocean. However, studying effectiveness of surfactants to fight hydrocarbon pollution in the open sea remains a challenge, and research is still ongoing in this area [10]. Much of the laboratory research points to the use of microbes in situ to produce surfactants. An alternative method to harness *B. subtilis* could be to produce Surfactin under optimal industrial conditions, transport it to the site of plastic pollution, and spray it to stimulate biodegradation.

Studying formulations that are inherently more vulnerable to biodegradation and promoting the use of such plastics can help with the natural degradation process. Research shows that additives such as pro-oxidants and starch make plastics biodegradable [11]. For *B. subtilis* to be a practical option to tackle the enormous amount of plastic waste, it should be deployable at scale. Further experimentation is required to study the optimal methods to incubate, transport, and deploy large amounts of this bacterium, while also evaluating any potential adverse impact on the aquatic ecosystems when doing so.

REFERENCES

[1] Geyer, Roland, et al. "Production, Use, and Fate of All Plastics Ever Made." *Science Advances*, vol. 3, no. 7, 19 July 2017, doi:10.1126/sciadv.1700782.

[2] National Oceanic and Atmospheric Administration. "Can marine debris degrade on its own in the environment?" https://oceanservice.noaa.gov/facts/ degrade.html Accessed Feb 19, 2019

[3] Restrepo-Flórez, Juan-Manuel, et al. "Microbial Degradation and Deterioration of Polyethylene – A Review." International Biodeterioration & Biodegradation, Elsevier, 11 Jan. 2014, www.sciencedirect.com/ science/article/pii/S096483051300454X.

[4] Vimala. P and Lea Matthew. Biodegradation of Polyethylene using Bacillus subtilis. 2016. http://www.Sciencedirect.com/science/article/pii/S2212017316301153. Accessed October 3, 2018.

[5] Alshehrei, Fatimah. (2017). Biodegradation of Synthetic and Natural Plastic by Microorganisms. Journal of Applied & Environmental Microbiology. 5. 8-19.

[6] Borriss, Rainer, et al. "Bacillus Subtilis, the Model Gram-Positive Bacterium: 20 Years of Annotation Refinement." *Microbial Biotechnology*, John Wiley and Sons Inc., Jan. 2018, www.ncbi.nlm.nih.gov/pmc/articles/PMC5743806/.

[7] Yan, Nan, et al. "Influence of Salinity and Water Content on Soil Microorganisms." *International Soil and Water Conservation Research*, vol. 3, no. 4, 2015, pp. 316–323., doi:10.1016/j.iswcr.2015.11.003.

[8] Makkar, et al. "Optimization of Surfactin Production by Bacillus Subtilis Isolate BS5." *Applied Biochemistry and Biotechnology*, Humana Press Inc, 1 Jan. 1999, link.springer.com/article/10.1007/s12010-008-8155-x.

[9] "Understanding the Science of Ocean and Coastal Acidification." *EPA*, Environmental Protection Agency, 23 Aug. 2019, www.epa.gov/ocean-acidification/understanding-science-ocean-and-coastal-acidification.

[10] Freitas, Bruno G, et al. "Formulation of a Commercial Biosurfactant for Application as a Dispersant of Petroleum and By-Products Spilled in Oceans." Frontiers in Microbiology, Frontiers Media S.A., 18 Oct. 2016. www.ncbi.nlm.nih.gov/pmc/articles/PMC5067411/.

[11] Bonhomme, S, et al. "Environmental Biodegradation of Polyethylene." Polymer Degradation and Stability, Elsevier, 11 June 2003, www.sciencedirect.com/science/article/pii/S0141391003001290